J. Fluid Mech. (2012), *vol.* 691, *pp.* 594–604.
doi:10.1017/jfm.2011.516

Experimental investigation of nonlinear instabilities in annular liquid sheets

D. Duke†, D. Honnery and J. Soria

Laboratory for Turbulence Research in Aerospace and Combustion, Department of Mechanical and Aerospace Engineering, Monash University, Clayton, Victoria 3800, Australia

(Received 15 July 2011; revised 27 October 2011; accepted 20 November 2011)

The aerodynamically driven annular liquid sheet exhibits a complex nonlinear instability. Novel interfacial velocimetry experiments suggest that two distinct physical sources of instability may be present. The first is the well-known free shear layer instability, which is quasi-sinusoidal and nonlinear. The second is a distinct nonlinear rupturing instability, modulated on the previous one. It may be directly driving primary atomization. This instability has not been previously observed in isolation and is inherently nonlinear and non-sinusoidal. Novel application of Koopman analysis and the Hilbert transform permit investigation of these distinct instabilities. A greater understanding of the rupturing instability may lead to a better understanding of atomization phenomena.

Key words: gas/liquid flows, interfacial flows (free surface), nonlinear instability

1. Introduction

The aerodynamically driven annular liquid sheet exhibits a complex, nonlinear instability mechanism that convectively drives the primary atomization of the flow. This mechanism is poorly understood, a problem that is shared in part by many similar geometries such as planar sheets and jets (Lin & Reitz 1998; Eggers & Villermaux 2008; Balachandar & Eaton 2010).

Quantitative experimental measurements of annular sheets are particularly challenging due to the need for simultaneously high dynamic range and resolution in both space and time. Theory and modelling have therefore been the focus of a great deal of research, including many detailed linear stability analyses (Lin 2003). For simpler geometries, nonlinear stability analysis (Jazayeri & Li 2000) has shown some improved results, and such techniques are now being extended to annular geometries (Ibrahim & Jog 2008). Comparison with the relatively small body of existing empirical data is poor (Kawano *et al.* 1997; Adzic, Carvalho & Heitoyr 2001; Lozano *et al.* 2001). To better understand the nonlinear instability mechanism and assess theoretical modelling attempts appropriately, improved experiments are essential.

Empirical analysis has typically been limited to the taxonomy of large-scale structures apparent to the observer through high-speed photography (Kendall 1986; Li & Shen 2001) and the measurement of dominant frequency components (Kawano *et al.* 1997) without a great deal of physical interpretation. For solid jets, a more

† Email address for correspondence: daniel.duke@monash.edu

physically robust theory of a dual Kelvin–Helmholtz to Rayleigh–Taylor instability mechanism exists (Marmottant & Villermaux 2004), and it is likely that the annular sheet exhibits similar yet more complex physical phenomena. No measurements of the transient dynamics of these flows have yet been available to test such a theory.

Recent developments in high-speed digital imaging and quantitative velocimetry permit more highly resolved measurements of annular sheet instabilities (Duke, Honnery & Soria 2010, 2011*a*). Recent developments in Koopman analysis open the possibility of directly measuring the growth rates of these instabilities for the first time (Rowley, Mezić & Bagheri 2009; Schmid 2010, 2011).

With a significantly larger database of measurements available, we may propose a refined model for the formation of instabilities in annular sheets. This may challenge some of the implicit assumptions made in many modelling approaches. The first implicit assumption in many models is that a singular nonlinear instability evolves convectively, determined by both initial perturbations from the nozzle boundary layer and the dual-free shear layer of the annular sheet (Kim & Sirignano 2000). The second implicit assumption is that the instabilities may be considered sinusoidal or part of a sine series (Barlow, Helenbrook & Lin 2010). Thirdly, linear stability analyses assume that the flow has a linearly receptive region very near the nozzle, which has a bearing on whether the flow downstream will be unstable.

In this paper we present novel highly resolved velocity measurements of the interfacial velocity of an aerodynamically driven annular liquid sheet. We propose that two distinct instability sources are present, rather than one. We take measurements of their growth rates for the first time. The instabilities are completely nonlinear within the dynamic range of measurement. A new rupturing instability is observed to be modulated on the upstream instabilities rather than evolving from them. It is distinctly nonlinear and non-sinusoidal. Relationships between the growth rates and frequency components of each source of instability are investigated. The nature of these instabilities may indicate the need to re-think theoretical approaches to these flows.

2. Method

2.1. *Experiment set-up*

The annular nozzle is shown in figure 1. A series of perforated plates and settling screens produce a uniform turbulence intensity, and a contraction of the liquid and outer air annuli reduces boundary layer thickness. The inner nozzle has a slight expansion. Air is delivered to the separately metered inner and outer co-flowing air jets from a regulated source, and a recirculation pump provides a constant water flow velocity to generate the liquid sheet. Hot-wire anemometry of the gas co-flows shows that the air flow is purely axial (no swirl), exhibits a top-hat profile and is steady (Duke *et al.* 2010).

The sheet thickness in this study is $h = 1.5$ mm. The liquid sheet is thus characterized by the well-known Reynolds and Weber numbers,

$$Re = \overline{U}_w h/\nu_w, \tag{2.1a}$$

$$We = \rho_w \overline{U}_w^2 h/\sigma, \tag{2.1b}$$

where subscripts i, o and w represent the inner and outer gas co-flows and the liquid sheet, respectively, and σ is surface tension. The gas co-flows are characterized by the shear velocity deficit of the mean velocity of the bulk flow normalized by liquid

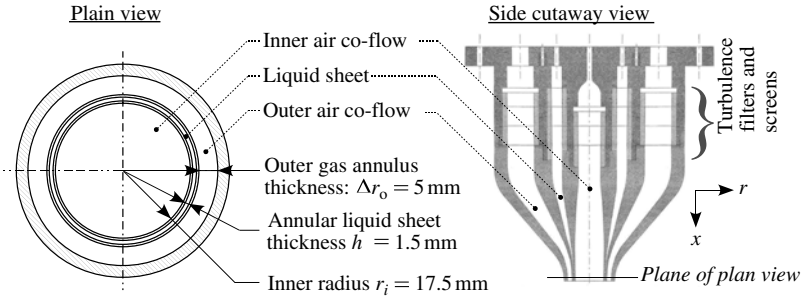

FIGURE 1. Annular nozzle geometry. A plan view of the nozzle at the exit plane and a cutaway view of the axisymmetric nozzle are shown. The outer gas and liquid sheet annuli have contractions of 4.6:1 and 7.3:1, respectively. The inner gas co-flow has an expansion of 1.3:1. Nozzle diagram reproduced with permission (Wahono *et al.* 2008).

velocity,

$$\Delta \overline{U}'_{i,o} = (\overline{U}_{i,o} - \overline{U}_w)/\overline{U}_w, \tag{2.2}$$

where $\overline{U}$ is measured using the mass flow rate and nozzle exit plane geometry. Variations in back-pressure and temperature for both air and water flows are taken into account.

The outer gas–liquid interface is imaged via line of sight using a back-lit strobed light-emitting diode (LED) array and high-speed PCO DIMAX camera operating at 7500 frames s^{-1} with a spatial resolution of 48 pixels mm^{-1}. We are not able to image the inner surface of an annular sheet, and the measurements in this paper are conditional on the outer sheet surface. In this study, only flow conditions in which instability is driven from the outer sheet surface are considered in the Koopman analysis. The inner gas velocity ratio is set to $\Delta U'_i = 0$.

2.2. *Correlation velocimetry*

High-speed digital images of the gas–liquid interface are analysed using a subpixel correlation image velocimetry algorithm. A complete error analysis and further details can be found in Duke *et al.* (2010, 2011*a*). The correlation fitting function is optimized for the interfacial profile. Uncertainty in velocity measurement is estimated by sensitivity analysis to be $\pm 0.085\overline{U}_w$.

The image depth of field is small, focusing only on the tangent profile of the outer interface. Line-of-sight measurement captures the surface velocity $u(x, t)$ as a function of both time (t) and axial distance (x). The surface instabilities of the axial annular sheet are known to be dominantly axisymmetric (Li & Shen 1999; Duke *et al.* 2010). The azimuthal component is negligible and only the radial velocity component is of interest.

Over 57 000 continuous frames are captured per experiment, giving 5.7×10^7 instantaneous measurements at 1000 discrete axial positions. Measurements are at least an order of magnitude more finely resolved compared to previous studies (Kawano *et al.* 1997; Adzic *et al.* 2001; Li & Shen 2001). Relative to the instability, resolution is typically 75 samples per wavelength in x and 150 samples per period in t.

Velocity is scaled by the mean sheet velocity, and may also be normalized by root mean square (r.m.s.),

$$u'(x,t) = u(x,t)/\overline{U}_w, \tag{2.3a}$$

$$\hat{u}(x,t) = u'(x,t)/u'_{rms}. \tag{2.3b}$$

2.3. *Diagnostic techniques*

A spectral analysis is performed by taking the fast Fourier transform (FFT) of $u'(x_i,t)$ with a sliding Hann window. Each spectrum is made up by 55 000 FFTs. The spectral density is normalized by the variance of u'. The rate of change of spectral density with x/h integrated over a frequency band may then approximate the growth rate of a predominantly sinusoidal instability within that band (Duke *et al.* 2010). A spectral analysis cannot measure the transient properties of broadband nonlinear instabilities. To extract the growth or decay rates of transient convective instabilities, a new approach is taken using the Koopman modes of $u(x,t)$. Modes are calculated via the dynamic mode decomposition (DMD) algorithm of Schmid (2010). As the flow is known *a priori* to be convectively unstable in the axial (x) coordinate, DMD in x permits extraction of the complex stability plane of u.

We have recently undertaken a parametric synthetic error analysis of the DMD technique. It provides an estimate of the numerical error introduced in the growth rate as a function of data quantity, quality and waveform (Duke, Soria & Honnery 2011*b*). Error has been shown to be a function of growth rate and waveform, when the data quantity and signal-to-noise ratio are fixed. Sawtooth and square waveform types have been shown to be an order of magnitude less accurately measured than sinusoidal waves under similar conditions. Using this approach, a parametric error function may estimate the numerical error expected in the growth rate (γ) from experimental data, as a function of the measured γ and the waveform profile. Numerical error may range from 10^{-5} up to an order of magnitude larger than γ depending on the conditions. In the present study, the upper error for γ in the near-nozzle region is $\pm 20\,\%$.

Transient properties can also be investigated by phase averaging $u'(x,t)$, conditional on a fixed or locally variable frequency. The former is determined by the FFT peak frequency, and the latter is determined by permitting frequency modulation of $\pm 50\,\%$ around the peak, using local maxima to determine the frequency. Where multiple modulated instabilities may be present, the Hilbert transform provides a convenient tool for demodulating these instabilities (Huang *et al.* 1996). The phase shifting of a dominant 'carrier' wave instability permits its cancellation, leaving only the modulated signal,

$$u'_{\mathscr{H}}(x_i,t) = \left|\mathscr{H}(u'(x_i,t))\right|, \tag{2.4}$$

where $\mathscr{H}$ is the complex Hilbert operator. The 'carrier' wave itself may also be extracted,

$$u'_{\mathscr{C}}(x_i,t) = \frac{u'(x_i,t)}{u'_{\mathscr{H}}(x_i,t) + \alpha}, \tag{2.5}$$

where α is a constant to reduce the effects of noise amplification from $u'_{\mathscr{H}}$ through to $u'_{\mathscr{C}}$ as $|u'_{\mathscr{H}}| \to 0$. Our measurements are optimized for $\alpha = 0.1\overline{U}_w$. The Koopman modes of $u'_{\mathscr{H}}$ and $u'_{\mathscr{C}}$ thus permit a novel calculation of the growth rates of modulated instabilities in isolation.

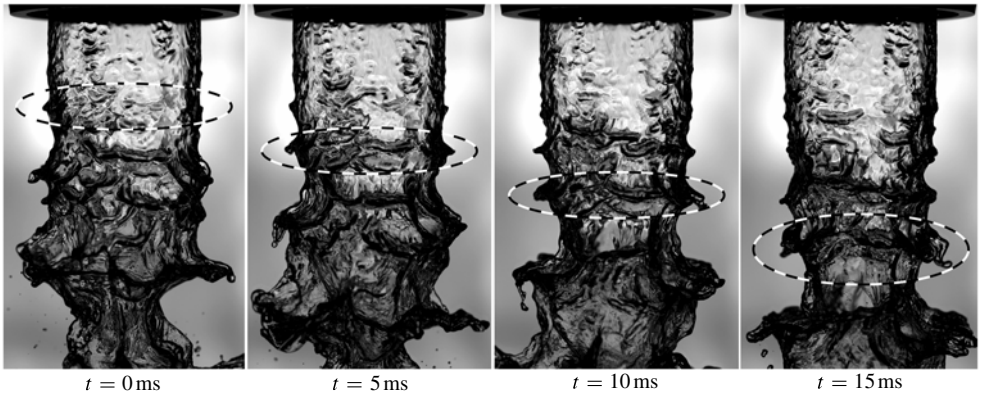

FIGURE 2. A sequence of still images showing a typical convective instability (indicated by the oval) at $Re = 2400$, $We = 60$, $\Delta\overline{U}_i = 0$ and $\Delta\overline{U}_o = 11.3$. The sheet diameter is 38.8 mm.

All calculations were performed using in-house MPI parallelized C++ codes. The open-source CImg, ARPACK, LAPACK and BLAS libraries were used. Parallel computations were done on the Monash Sun Grid and at the NCI National Facility.

3. Results and discussion

A typical convective instability is shown in figure 2. High-speed movies are also available online (http://youtu.be/XOvk6NumQkw). At higher *Re*, instabilities are more easily observed owing to their longer development distance. A small perturbation near the nozzle grows until it is pulled away from the bulk flow and becomes a ligament – the beginning of primary atomization. By observation, the assumption that a single instability evolves as it convects downstream appears reasonable – the evolution is smooth and repetitive. The instability is evolving nonlinearly once it is far enough away from the nozzle, and there may be a linear region close to the nozzle that cannot be directly observed. However, more detailed investigation of these instabilities in streamwise space and time reveals that many of the above observations are not physically correct.

3.1. *Spectral analysis of near-nozzle region*

Figure 3 indicates typical power spectra of the interfacial velocity time series as a function of both $\Delta\overline{U}_o'$ (figure 3*a*) and *Re* (figure 3*b*). A singular dominant frequency is observed due to the oscillation of the free shear layer. We have previously demonstrated that the peak remains constant with x/h (Duke *et al.* 2010). The effect of increasing *Re* significantly increases the frequency of the peak as compared to $\Delta\overline{U}_o'$, even though the momentum ratio of the gas to liquid decreases as *Re* increases. However, figure 3(*a*) indicates that without a relatively high outer gas flow ratio the shear layer instability does not form (no frequency peak appears). This suggests that the formation of an instability in the dominant free shear layer requires a momentum contribution from the outer gas flow in order to grow.

3.2. *Koopman mode analysis and Hilbert transformation*

Beyond the near-nozzle region ($x/h > 3$), the instabilities rapidly become non-sinusoidal but tend to sawtooth waves as shown in figure 4(*a*). At this point, the

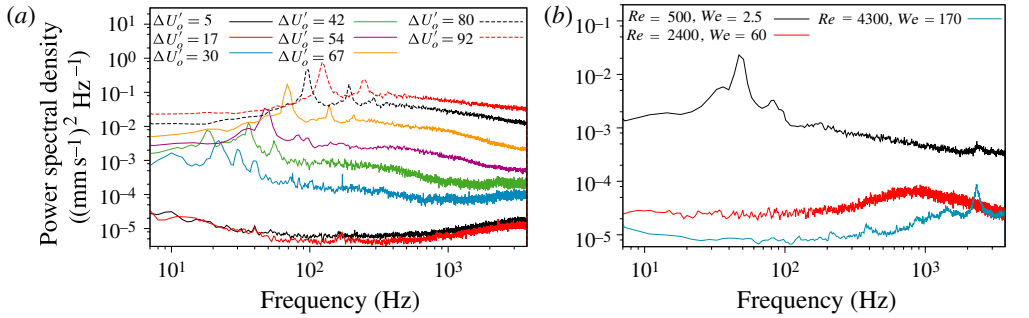

FIGURE 3. Power spectra from Fourier transforms of u' versus: (*a*) $\Delta\overline{U}_o'$, at $Re = 500, We = 2.5$, $\Delta\overline{U}_i' = 0$; and (*b*) Re, at $\Delta\overline{U}_i' = 0$, $\Delta\overline{U}_o' = 54$.

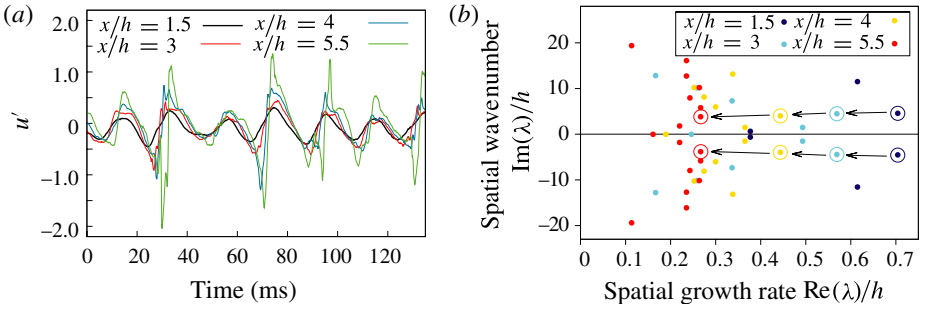

FIGURE 4. Time-series and Koopman modes of u' at $Re = 500$, $We = 2.5$: (*a*) time series of u', showing the sinusoidal to pseudo-sawtooth transition with increasing x; (*b*) spatial Koopman eigenvalue spectra of u'. Leading modes are indicated by larger points. Their path in the complex plane as x/h increases is indicated by arrows.

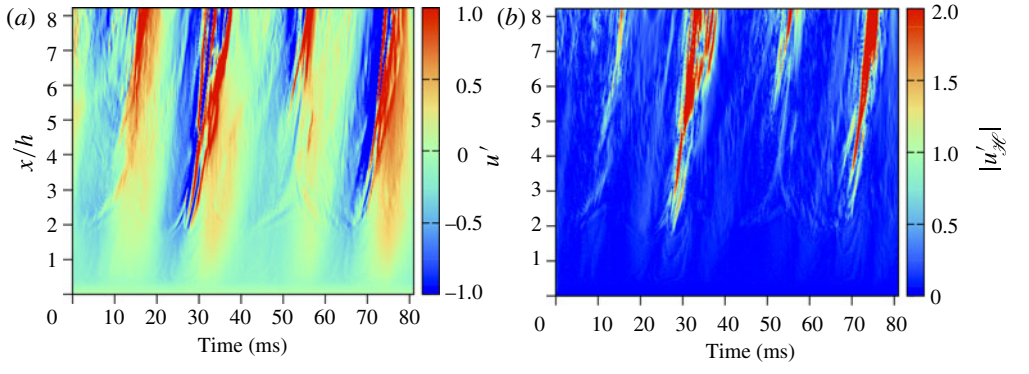

FIGURE 5. Space-time contours of u' at $Re = 500$, $We = 2.5$: (*a*) the directly measured velocity u' and (*b*) the magnitude of the complex Hilbert transform $|u'_{\mathscr{H}}|$ are compared, well upstream of breakup. Only a very small segment of the overall time domain for a single time series is shown. The sheet breakup occurs for $x/h \in [10, 15]$, by which time the rupturing instability has overtaken the shear layer instability fully.

instability is due to a double-free multiphase shear layer and exhibits a well-known flapping behaviour (Kawano *et al.* 1997). For the following analysis, all figures relate to measurements at $Re = 500$, $We = 2.5$, $\Delta\overline{U}_i = 0$ and $\Delta\overline{U}_o = 54$. The liquid sheet velocity is $U_l = 0.35$ m s^{-1}.

DMD of u' in the x dimension permits extraction of the growth rates of unstable convective Koopman modes as shown in figure 4(*b*). Growth rate γ is exponential growth, and thus the amplitude is proportional to $e^{\gamma x}$. The use of exponential notation facilitates comparison with linear stability analysis and is the conventional representation for the complex stability plane. The leading modes of u' have an unstable complex conjugate pair whose γ reduces as x/h increases, indicating nonlinear, quasi-sinusoidal instability. The number of unstable modes increases as x/h increases and the peak γ reduces, indicating that the instabilities become less sinusoidal as they evolve. The corresponding wavenumber remains relatively constant (consistent with spectral analysis).

A small segment of the velocity field is shown in figure 5(*a*). The sinusoidal shear layer instability is visible in the near-nozzle region $x/h < 3$. The rupture and initial breakup of the sheet are clearly visible as disruptions that grow for $x/h > 3$. These rupturing instabilities may not be due to evolution of the more sinusoidal free shear layer instability, but appear to be modulated onto them and conditional on their frequency. This suggests that, whilst a frequency analysis of the initial instability may lead to a reasonable estimate of the frequency of the rupturing and ligament formation, their growth rates may not be related.

Through the Hilbert transformation, this rupturing instability may be demodulated from the free shear layer instability so that its growth rate may be separately measured. Figure 5(*a*) is transformed into figure 5(*b*). The rupturing instability is isolated well.

The DMD eigenvalues of u', its Hilbert transform $u'_{\mathscr{H}}$ and the subtracted carrier $u'_{\mathscr{C}}$ are shown in figure 6(*a*). At $x/h = 3$, the rupturing instability is growing more rapidly than its 'carrier' wave. In our application, the 'carrier' is the free shear layer instability evident in the near-nozzle region.

The phase average profile of u' is shown in figure 6(*b*). The frequency is conditional on the upstream turbulence of the nozzle boundary layer and the free shear layer, and as such it is observed to vary slightly. This can also be quantified by the width of the spectral peak in figure 3. The modulated rupturing instability of $u'_{\mathscr{H}}$ is evident at zero phase as a spike that rapidly protrudes from the 'carrier'.

A rupturing mechanism is observed in figure 2. At $t = 5$ ms the instability begins to peel from the bulk of the liquid. An impression is created upstream of the wave crest by the faster-moving outer airflow. Between figures 2 and 6(*b*), a physical explanation for the birth of the sheet rupturing instability may be proposed. The instability occurs in a consistent position in phase space, typically every two periods. This corresponds to the negative-velocity part of the wave, where a large positive-velocity spike begins to grow. Physically, this represents the surface moving inwards as the instability moves outwards. Figures 2 and 6(*b*) also show the instability being pulled away.

When the sheet is expanding, surface tension counteracts its motion and slows it. When contracting, surface tension acts in concert and accelerates the sheet. Part of the wave crest is 'left behind' and is convected downstream by the fast-moving outer airstream at a greater speed than the base of the wave. This very rapidly distorts the wave in a nonlinear but consistent manner and is very similar to the 'surface-stripping' behaviour of solid jets (Marmottant & Villermaux 2004). The change in group velocity is evident from the orientation of the structures in figure 5. This

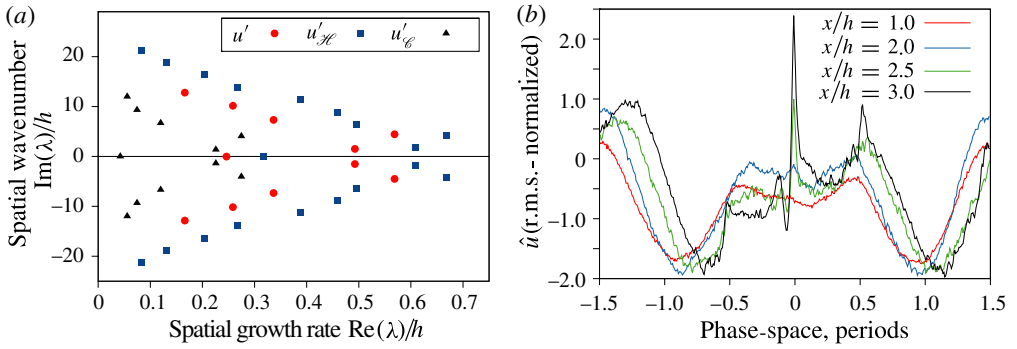

FIGURE 6. Transient properties of the velocity time series: (*a*) comparison of the leading Koopman eigenvalues of u', $u'_{\mathscr{H}}$ and $u'_{\mathscr{C}}$ at $x/h = 3$, $Re = 500$, $We = 2.5$; (*b*) phase average function of u' at $Re = 500$, $We = 2.5$ with variable instantaneous frequency versus x/h. A sharp spike appears at zero phase as x/h increases.

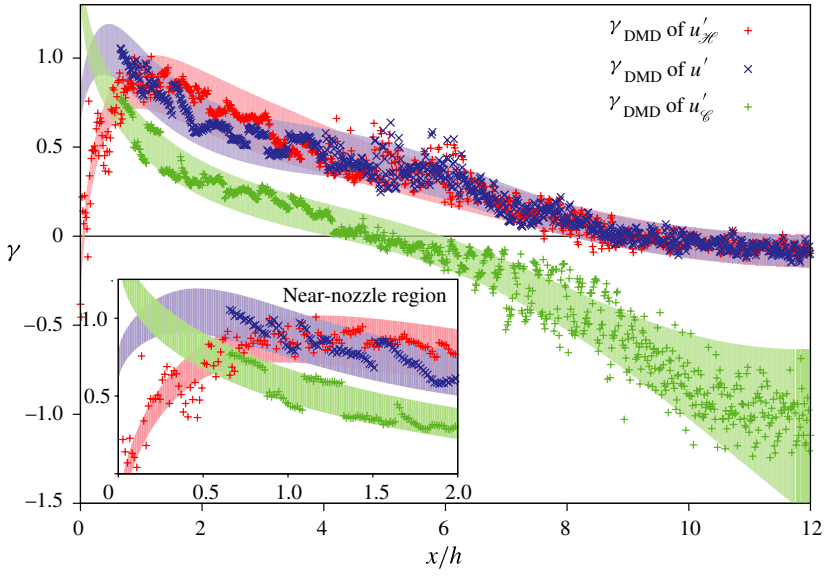

FIGURE 7. Comparison of DMD growth rates versus x/h for u' (blue $\times$), $u'_{\mathscr{H}}$ (red $+$) and $u'_{\mathscr{C}}$ (green $+$) at $Re = 500$, $We = 2.5$. The shaded band for each set of markers is the predicted uncertainty in γ from synthetic analysis around the moving average. Inset: near-nozzle region, $x/h < 2$.

instability is entirely due to surface tension-driven discontinuities and nonlinearities and will not be captured in a typical stability analysis.

3.3. *Spatial variation of growth rates*

In order to map the effect of varying growth rate shown in figure 4(*b*), we apply a sliding window to u', $u'_{\mathscr{H}}$ and $u'_{\mathscr{C}}$. The window width is 2.5 h, and as such the growth rates indicated can be considered a best linear fit to the amplification over ± 1.25 h. The width of the sliding window is selected as a trade-off between spatial smoothing and accuracy in γ, as indicated by error analysis (Duke *et al.* 2011*b*).

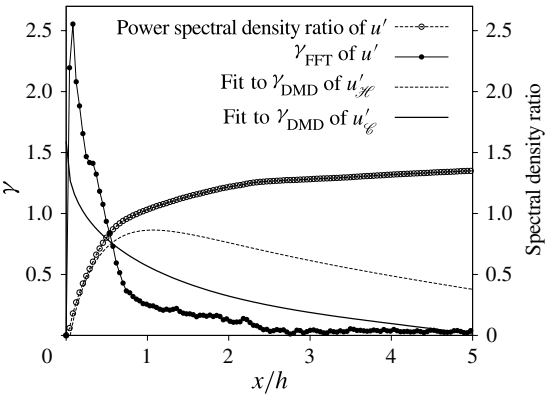

FIGURE 8. Comparison of growth rate profiles from DMD and FFT approaches at $Re = 500$, $We = 2.5$.

Figure 7 shows for the first time the nonlinear spatial variation in γ for this flow at one condition. An uncertainty band is calculated from a synthetic wave analysis using the known data quantity, quality, measured growth rate and an estimate of the local waveform shape (Duke *et al.* 2011*b*). Here the error functions for sine waves and sawtooth waves are both used, with a linear taper from one to the other over the near-nozzle development length of $0 < x/h < 3$. This uncertainty is added to a moving average of the DMD measurements (the similarly coloured markers), which is a sixth-order polynomial fit to the data. Any points that fall outside this uncertainty band are deviations, which cannot be explained by experimental uncertainty or the numerical error in the DMD.

For u' and $u'_{\mathscr{H}}$, the flow shows increasing instability up to a turning point around $x/h \approx 1$, and a continuing decline in γ thereafter. The carrier (the sinusoidal free shear layer instability) is observed to start at a high γ and then declines downstream, becoming stable for $x/h \geqslant 6$. At this point the flow is entirely controlled by the rupturing instability and no part of the original shear layer instability remains. The rupturing instability remains unstable but asymptotes to marginal stability as the flow atomizes.

Figure 8 compares γ for both spectral and DMD approaches. The spectral density follows the least-squares fit for $u'_{\mathscr{H}}$, but diverges past the turning point. The growth rate calculated from its gradient is much higher closer to the nozzle than DMD, does not show a turning point and is lower downstream. It follows a similar profile to $u'_{\mathscr{C}}$, as the Hilbert carrier is the dominant flapping frequency.

Figures 7 and 8 demonstrate that the flow is fully nonlinear and does not exhibit a visible linear region. The greatest nonlinearities occur in the near-nozzle region. Figures 4(*a*) and 6(*b*) show that the rupture is also non-sinusoidal. The conditions under which it forms determine its frequency, i.e. the frequency of the free shear layer instability. However, the spectral growth rates are non-physical. If they were accurate, the flow would atomize explosively in the near-nozzle region, which is not corroborated by experiments. Koopman modes may capture nonlinear broadband instabilities more accurately.

4. Conclusions

Annular liquid sheets are shown to be driven by two instabilities: the free shear layer instability, and a newly observed rupturing instability. The first creates the conditions for the birth of the second and determines some but not all of its properties. Momentum is supplied primarily by the shear at the gas–liquid interface, creating the well-known quasi-sinusoidal shear layer instability in the near-nozzle region. Rupturing instabilities occur at a point in the phase cycle of the shear layer instability where the sheet is retracting inwards and the surface is peeled away by the faster-moving gas. Rupturing and ligament formation frequencies are strongly controlled by the upstream instabilities but their growth rates may be unrelated. Rupturing instabilities begin well upstream of breakup; by the time the sheet breaks, the rupturing instability dominates the flow.

Previous studies have revealed the peak frequency component of the free shear layer instability, but a rupturing instability is measured here for the first time. Growth rates of instabilities reduce as the flow convects downstream after a turning point in the near-nozzle region, but remain positive up to breakup. The complete nonlinearity of the flow implies that linear stability analysis is never sufficient for these flows. Variation between DMD and spectral growth rates suggest that the instability has a wide bandwidth but is sinusoidal in the near-nozzle region. The rupturing instability, which may directly drive the formation of ligaments and the primary breakup process, is distinctly non-sinusoidal and this may have further implications for nonlinear modelling and spectral techniques.

Instabilities in the boundary layer inside the nozzle, which have not been measured, may have additional effects. Furthermore, complex parametric effects will probably occur over the space of Re, We, $\Delta U_{i,o}$ and sheet geometry beyond those considered in this paper. A more expansive parametric analysis and a more detailed comparison with existing theory will be the subject of a forthcoming paper.

Acknowledgements

The authors wish to acknowledge the support of the Australian Research Council. The first author was supported by an Australian Postgraduate Award whilst undertaking the study. The authors also wish to acknowledge the support of the NCI National Facility, the Monash Sun Grid and the Monash Large Research Data Store for the provision of cluster computing resources.

REFERENCES

ADZIC, M., CARVALHO, I. & HEITOYR, M. V. 2001 Visualization of the disintegration of an annular liquid sheet in a coaxial airblast injector at low atomising air velocities. *Opt. Diagnost. Engng* **5** (1), 27–38.

BALACHANDAR, S. & EATON, J. K. 2010 Turbulent dispersed multiphase flow. *Annu. Rev. Fluid Mech.* **42** (1), 111–133.

BARLOW, N. S., HELENBROOK, B. T. & LIN, S. P. 2010 Transience to instability in a liquid sheet. *J. Fluid Mech.* **666**, 358–390.

DUKE, D., HONNERY, D. & SORIA, J. 2010 A cross-correlation velocimetry technique for breakup of an annular liquid sheet. *Exp. Fluids* **49**, 435–445.

DUKE, D. J., HONNERY, D. & SORIA, J. 2011*a* A comparison of subpixel edge detection and correlation algorithms for the measurement of sprays. *Intl J. Spray Comb. Dyn.* **3** (2), 93–110.

DUKE, D., SORIA, J. & HONNERY, D. 2011*b* An error analysis of the dynamic mode decomposition. *Exp. Fluids*, doi:10.1007/s00348-011-1235-7.

EGGERS, J. & VILLERMAUX, E. 2008 Physics of liquid jets. *Rep. Prog. Phys.* **71** (3), 036601.

HUANG, N. E., SHEN, Z., LONG, S. & WU, M. 1996 The empirical mode decomposition and the Hilbert spectrum for nonlinear and non-stationary time series analysis. *Proc. R. Soc. Lond.* A **454**, 903–995.

IBRAHIM, A. & JOG, M. 2008 Nonlinear instability of an annular liquid sheet exposed to gas flow. *Int. J. Multiphase Flow* **34** (7), 647–664.

JAZAYERI, S. & LI, X. 2000 Nonlinear instability of plane liquid sheets. *J. Fluid Mech.* **406**, 281–308.

KAWANO, S., HASHIMOTO, H., TOGARI, H. & IHARA, A. 1997 Deformation and breakup of an annular liquid sheet in a gas stream. *Atomiz. Sprays* **7**, 359–374.

KENDALL, J. 1986 Experiments on annular liquid jet instability and on the formation of liquid shells. *Phys. Fluids* **29** (7), 2086–2094.

KIM, I. & SIRIGNANO, W. 2000 Three-dimensional wave distortion and disintegration of thin planar liquid sheets. *J. Fluid Mech.* **410**, 147–183.

LI, X. & SHEN, J. 1999 Experimental study of sprays from annular liquid jet breakup. *J. Propul. Power* **15** (1), 103–110.

LI, X. & SHEN, J. 2001 Experiments on annular liquid jet breakup. *Atomiz. Sprays* **11**, 557–573.

LIN, S. P. 2003 *Breakup of Liquid Sheets and Jets*. Cambridge University Press.

LIN, S. P. & REITZ, R. 1998 Drop and spray formation from a liquid jet. *Annu. Rev. Fluid Mech.* **30**, 85–105.

LOZANO, A., BARRERAS, F., HAUKE, G. & DOPAZO, C. 2001 Longitudinal instabilities in an air-blasted liquid sheet. *J. Fluid Mech.* **437**, 143–173.

MARMOTTANT, P. & VILLERMAUX, E. 2004 On spray formation. *J. Fluid Mech.* **498**, 73–111.

ROWLEY, C., MEZIĆ, I. & BAGHERI, S. 2009 Spectral analysis of nonlinear flows. *J. Fluid Mech.* **641**, 115–127.

SCHMID, P. J. 2010 Dynamic mode decomposition of numerical and experimental data. *J. Fluid Mech.* **656**, 5–28.

SCHMID, P. J. 2011 Application of the dynamic mode decomposition to experimental data. *Exp. Fluids* **50** (4), 1123–1130.

WAHONO, S., HONNERY, D., SORIA, J. & GHOJEL, J. 2008 High-speed visualisation of primary break-up of an annular liquid sheet. *Exp. Fluids* **44** (3), 451–459.